Materials Chemistry Horizons RESEARCH

Magnetic Nanocomposite Hydrogel based on Arabic Gum for Remediation of Lead(II) from Contaminated Water

Fereshte Hassanzadeh-Afruzi, Golnaz Heidari, Ali Maleki*

Catalysts and Organic Synthesis Research Laboratory, Department of Chemistry, Iran University of Science and Technology, Tehran 16846-13114, Iran

Corresponding author: maleki@iust.ac.ir (A.Maleki)

Mater. Chem. Horizons, 2022, 1(2), 107-122 10.22128/mch.2022.570.1013 OPEN ACCESS

ABSTRACT

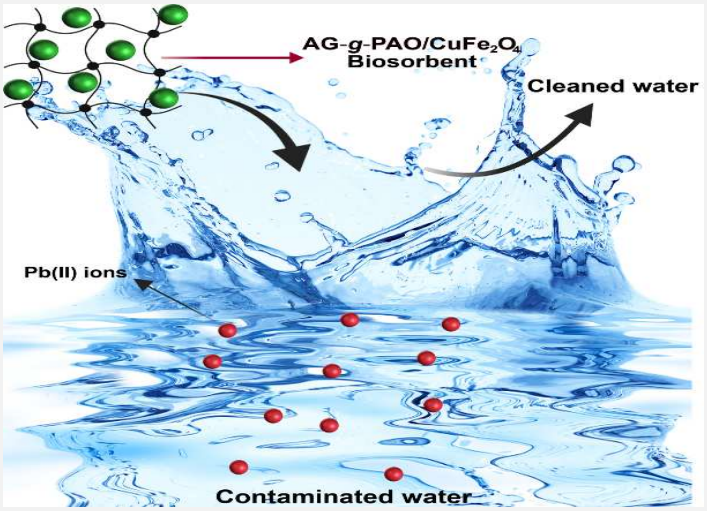

A new organic/inorganic biosorbent hydrogel consisting of Arabic gum (AG), polyamidoxime(PAO), and $CuFe_2O_4$ was synthesized by the grafting copolymerization method. The first step was the preparation of $CuFe_2O_4$ magnetic nanoparticles by the coprecipitation method. Next, using a crosslinker and a radical initiator, acrylonitrile was grafted onto Arabic gum (AG) in the existence of $CuFe_2O_4$ nanoparticles to produce Arabic gum-*g*-polyacrylonitrile/$CuFe_2O_4$ (AG-*g*-PAN/$CuFe_2O_4$) nanocomposite hydrogel. In the last step, the acrylonitrile groups in the nanocomposite hydrogel were modified using hydroxylamine hydrochloride to obtain Arabic gum-*g*- polyamidoxime/$CuFe_2O_4$ (AG-*g*-PAO/$CuFe_2O_4$) nanocomposite hydrogel. X-ray diffraction (XRD), scanning electron microscopy image (SEM), fourier transformed infrared (FT-IR), energy-dispersive X-ray analysis (EDX), carbon-hydrogen-nitrogen (CHN) analysis, zeta potential, and Brunauer-Emmett-Teller (BET) analyses. vibrating sample magnetometer (VSM) and thermogravimetric analysis (TGA) were used to characterize the produced nanocomposite. The adsorption effectiveness of AG-*g*-PAO/$CuFe_2O_4$ for the removal of Pb(II) from aqueous solutions was investigated under various experimental settings, including starting Pb(II) concentration, contact time, adsorbent dose, and pH. The Langmuir isotherm model accurately categorized the experimental adsorption data, and the maximum adsorption capacity (Q_{max}) of the produced biosorbent for Pb(II) was determined to be 192.30 mg/g. The pseudo-second-order model suited the adsorption kinetic data well. Additionally, after three consecutive cycles, the AG-*g*-PAO/$CuFe_2O_4$ can be successfully reused without a significant loss in adsorption performance.

Keywords: Organic/inorganic nanocomposite hydrogel, Arabic gum, polyamidoxime, graft copolymer, lead(II) removal

1. Introduction

The use of freshwater has grown in modern civilizations, while per-capita water access has decreased. The quality of available water resources, on the other hand, is deteriorating owing to increased industrial activity, agriculture, inappropriate agricultural irrigation, increased production, ineffective municipal waste management, and a general disregard for water resource management [1-3]. Heavy metal ions, dyes, radioactive materials, pesticides, drugs, degradable waste, nitrates and phosphates, sediments, heat, and fluoride are known pollutants in water resources [1, 4-6]. Metal processing, mining, textile, battery production, plating, oil refining, paint manufacturing, pesticides, tanning, paper, pigment and paint production, printing, and photography are the sources that discharge heavy metals

Received: June 25, 2022
Received in revised: July 22, 2022
Accepted: August 12, 2022

to the environment and water resources [3]. The discharging of this type of contaminant into aquatic ecosystems, due to non-biological degradation, high toxicity, intrinsic persistence, and their bioaccumulation and biomagnification in nature especially in the food chain cause significant anomalies and problems in human health and quality of life of other species [7].

Arsenic, cadmium, chromium, lead, and mercury is the common heavy metals pollutants. Lead, highly toxic metal ions, can cause serious health problems for instance anemia, mental deficiency, brain damage, anorexia, vomiting, and malaise in humans. According to Environmental Protection Agency, the maximum acceptable level for lead in drinking water is 0.015 mg/ L. Therefore, the removal of these heavy metals before discharging contaminated effluents into water sources was essential to protect the health of aquatic lives, animals, humans, and the environment. Scientists have presented various methods such as membrane filtration, electrochemical, solvent extraction photocatalysis, chemical precipitation, ion exchange, coagulation-flocculation, and adsorption for water treatment. The methods mentioned above, despite their benefits such as rapid process, and being feasible on a lab scale, suffer from significant drawbacks on a large scale, for example, the formation of concentrated sludge or byproducts, high energy costs, and high-tech equipment [2, 4]. Adsorption has gained popularity due to its several advantages, including selectivity, ease of operation, excellent performance, and the ability to use a wide range of cost-effective materials as adsorbents and regeneration [8, 9]. Due to its positive characteristics such as natural resources, low cost, affordability, minimal environmental impact, stability, uptake rate, reusability, adsorption capacity minimal toxicity to living cells, fair costs, and availability, biopolymer-based adsorbents have been widely used as an ecologically friendly adsorbent to remove water contaminants [10, 11]. A great number of polysaccharides was utilized in the construction of polysaccharide-based adsorbent. Various gums such as guar gum[12], gum karaya[9, 13], xanthan gum[14], gum ghatti[15], and gum tragacanth[16] as part of natural polymers with outstanding capability for hydrogel-forming, contributed to the gum-based hydrogels construction[14]. The hydrogel is a three-dimensional homopolymer or copolymer network compound. This soft and wet material with high swelling, high water absorption capacity without dissolving, and flexible shape could provide metal ions with diffusion into its 3D network and subsequently stimulate interaction between diffused metal ions in contaminated water and surface functional groups on hydrogel [17, 18]. Arabic gum (AG), commonly known as acacia gum, is derived from specific acacia tree species. Based on the source, the chemical and physical properties and the composition percentage of the constituent components could fluctuate somewhat [19]. In general, about 97% of this compound is polysaccharides, and a very small portion of it, about 3%, is made up of protein units. The main chain of this natural polymer consists of galactopyranose units linked by β (1,3)-glycosidic bond. The side chains are mostly made up of two to five β-(1,3)-linked galactopyranosyl units that are linked to the linear chain through β-glycosidic connections (1,6). Apart from galactose, glucuronic acid, rhamnose, arabinose, and methyl glucuronic acid monomers are also present in the main backbone and branches [20, 21]. The AG is a sophisticated neutral or slightly acidic compound that is usually formed in a combination of calcium, magnesium, and potassium acidic salts, and as a result, it possesses a strong solubility in water [19].

Because of its physicochemical and structural qualities, this heteropolysaccharide has been widely used in a variety of industries. For its emulsifying, thickening, and stabilizing capabilities, this substance is used extensively in the food sector, such as in beverages, syrups, jellies, soft drinks, and ice cream formulation. It's also been employed in the textile industry, printing, medicines, and the creation of cosmeceuticals [22]. As mentioned, natural polymer-based hydrogel adsorbents have significant advantages, but reports indicate that the adsorption capacity of these unmodified adsorbents is not satisfied [14, 15]. Therefore much effort has been made to modify this material with diverse materials such as a silica-based nanoparticle, carbon-based compound, metal or metal oxide nanoparticle, polymers, and montmorillonite, to achieve efficient adsorbent with high adsorption capacity, heightened thermal and mechanical stability, or even magnetic recovery ability [9, 14]. The incorporation of magnetic nanoparticles in the network of a natural polymer-based hydrogel grafted by vinyl monomers could indeed bring an extra active adsorption site for efficient interaction with metal ions or another intended pollutant and thus enhance the absorption capacity. Furthermore, the combination of different materials results in a nanocomposite hydrogel with synergistic properties of compromising components. These kinds of materials have been the focus of research for the removal of heavy metal ions from wastewaters due to their characteristic properties, such as high surface area, suitable porosity,

biocompability, improved mechanical and thermal resistance, and high uptake rate. The literature survey demonstrated the efficiency of polysaccharide/and gum-based nanocomposite hydrogel toward heavy metal absorption, for example, Ghaemy and Sahraei reported the synthesis of modified gum tragacanth/graphene oxide composite hydrogel for adsorption of Pb(II), Cd(II), and Ag(I). The reported valus of adsorption capacity was about 142, 112 and 132 mg/g respectively. The experimntal data has followed the Langmuir model and pseudo-first-order kinetic model [16]. Yutang and et al. prepared the ethylenediaminetetra-acetic acid (EDTA) modified chitosan/polyacrylamide double network hydrogel and applied it for adsorption of heavy metal ions. The fabricated nanocomposite hydrogel showed excellent efficiency with theoretical maximum sorption capacities of 86.0, 99.4, and 138.4 mg/g for Cd(II), Cu(II), and Pb(II), respectively [17].

Recent research has shown that adsorbents containing nitrogen-containing functional groups as strong chelating ligands have been excellently able to remove heavy metals from aqueous solutions[23-26]. Given its great grafting efficiency and reactivity, polyacrylonitrile (PAN) could be grafted onto the backbone of natural polymers, allowing for additional chemical modifications [23, 27]. The current research used N, N-methylenebisacrylamide as a crosslinker, and ammonium persulfate as a radical initiator to create a novel organic/inorganic hydrogel based on grafted PAN onto the polymeric chains of AG in the existence of $CuFe_2O_4$ magnetic nanoparticles (MNPs). Using hydroxylamine hydrochloride, the produced magnetic hydrogel was then manipulated to convert the nitrile groups to amidoxime groups as bidentate ligands. Hence, the designed nanocomposite hydrogel with a combination of properties from natural polymer, synthetic polymer, and inorganic nanoparticles was applied as an effective adsorbent for Pb(II) removal from an aqueous solution. For this, The effects of important factors on adsorption capacity, i.e. metal ion starting concentration, contact duration, adsorbent dose, and pH were assessed. The residual concentration of Pb(II) after a contact time was measured by atomic absorption spectroscopy. Based on the experimental data, the Langmuir and Freundlich models were used to assess the adsorption isotherm, and the adsorption kinetic was studied by the pseudo-first and pseudo-second-order kinetic models. Then, the AG-g-PAO/$CuFe_2O_4$ adsorbent regeneration was explored well several times.

2. Experimental

2.1. Materials and characterization

Hydroxylamine hydrochloride, *N*, *N′*-methylene bisacrylamide (MBA), acrylonitrile (AN), and Arabic gum (AG) were provided by Sigma Aldrich Company. NaOH, $Fe(NO_3)_2.9H_2O$, $Cu(NO_3)_2.3H_2O$, $Pb(NO_3)_2$, ammonia solution (NH_4OH 28%), ammonium persulfate (APS), and all solvents were supplied from the Merck Company. FT-IR spectra were obtained by KBr pellets on a Shimadzu 8400 S spectrometer. The samples were analyzed for elements using energy-dispersive X-ray analysis (EDX) on a Numerix JEOL-JDX 8030 (30 kV, 20 mA). An X-ray diffractometer was used to acquire sample X-ray diffraction (XRD) patterns (Bruker D8 Advance). A scanning electron microscope (SEM, VEGA2 TESCAN) was used to examine the materials' morphology. A vibrating sample magnetometer (VSM) analysis was used to determine the magnetic properties of the samples. Thermogravimetric analysis (TGA) was used to investigate the thermal stability of materials with a BAHR-STA 504 instrument. The pH was adjusted using a PHS-3C pH meter. A flame atomic absorption spectrophotometer (AAS) was used to determine the concentration of Pb(II) in the mixture (Hewlett-Packard 3510).

2.2. Fabrication of AG-g-PAO/$CuFe_2O_4$ nanocomposite hydrogel

The nanocomposite hydrogel was prepared in three steps. In the first step the $CuFe_2O_4$ magnetic nanoparticles by the co-precipitation method according to reported literature [28]. In the next step, acrylonitrile was grafted onto Arabic gum (AG) in the presence of $CuFe_2O_4$ nanoparticles by N, N-methylenebisacrylamide as a crosslinker, and ammonium persulfate as a radical initiator to obtain Arabic gum-*grafted*-polyacrylonitrile/$CuFe_2O_4$ (AG-*g*-PAN/$CuFe_2O_4$) nanocomposite hydrogel [29]. In the third step, the acrylonitrile groups in the nanocomposite hydrogel were modified using hydroxylamine hydrochloride under the alkaline condition to obtain Arabic gum-*grafted*-polyamidoxime/$CuFe_2O_4$ (AG-*g*-PAO/$CuFe_2O_4$) nanocomposite hydrogel [30] (**Scheme 1**).

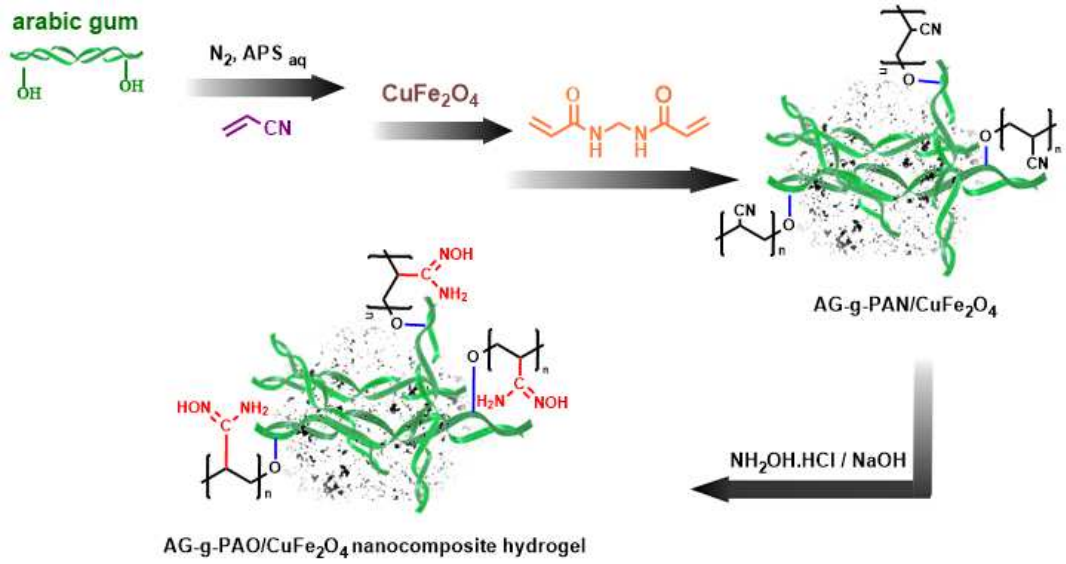

Scheme 1. Schematic preparation of AG-g-PAO/$CuFe_2O_4$ nanocomposite hydrogel.

2.3. Adsorption experiments

Many studies were conducted to determine the capacity of the AG-g-PAO/$CuFe_2O_4$ nanocomposite hydrogel to remove Pb (II) from aqueous solutions. The influence of key factors on adsorption capacities, such as starting Pb (II) concentration, contact duration, adsorbent quantity, and solution pH was investigated. To find the best medium pH, HCl (0.1 N) and NaOH (0.1 N) were used to alter the various pH levels in the range of 2 to 8. After that, different amounts of biosorbent from 5 mg to 20 mg and contact times from 30 to 120 min, and various initial Pb (II) concentrations in the range of 20-200 ppm, were examined to obtain optimum adsorption conditions. The adsorption isotherms were further investigated by referring the experimental results to the Freundlich and Langmuir models. The pseudo-first-order and pseudo-second-order models were also implemented to examine the adsorption kinetics. The experiments were done three times, with the average measured findings provided. The concentration of Pb(II) in the solution was determined using a flame atomic absorption spectrophotometer. The following equations were used to compute the adsorption efficiency (1) and capacity (2) of Pb(II) onto the AG-g-PAO/CuFe2O4 nanocomposite [10].

$$R\% = \left(\frac{C_i - C_e}{C_i}\right) \times 100 \quad (1)$$

$$Q_e = \left(\frac{C_i - C_e}{m}\right) \times V \quad (2)$$

The initial and equilibrium concentrations of Pb(II) in aqueous solutions (mg/L) are C_i and C_e, respectively. V is the solution volume (L) and m is the weight of the AG-g-PAO/$CuFe_2O_4$ biosorbent (g).

2.4. Desorption and reusability

50 mg of the AG-g-PAO/CuFe2O4-Pb complex was submerged in 0.2 M HCl and agitated for 1 hour at room temperature to study biosorbent desorption and recyclability. The biosorbent was subsequently separated from the acidic solution using a magnet. The concentration of liberated Pb(II) in the elution medium was then measured by AAS analysis. The percentage of desorption was calculated using the equation below [10].

$$\%D = \frac{A}{B} \times 100 \quad (3)$$

The mg of Pb(II) desorbed to the elution medium is A, while the mg of Pb(II) adsorbed on the AG-g-PAO/$CuFe_2O_4$ biosorbent is B. To re-use the separated biosorbent, it was sonicated in 50 mL distilled water and agitated at room temperature for about 1 hour, then collected using magnetic force, and finally dried and reused for more adsorption experiments.

3. Results and discussion

3.1. Characterization of adsorbent

The presence of the predicted functional groups was confirmed using FT-IR spectroscopy. **Figure 1** shows the FT-IR spectra of (a) AG, (b) AG-*g*-PAN/$CuFe_2O_4$, and (c) AG-*g*-PAO/$CuFe_2O_4$. The stretching vibration of the O-H bond of the carboxylic acid group and other hydroxyl groups is ascribed to a large absorption band in the region of 2500 to 3500 cm-1 in the FT-IR spectra of the AG [31]. The symmetric and asymmetric stretching vibrations of the aliphatic C-H bond are associated with two absorption bands at 2898 cm^{-1} and 2933 cm^{-1}, respectively [32, 33]. The stretching vibration of the COOH group's C=O bond is responsible for the intense absorption band at 1625 cm^{-1} [34]. The absorption bands in the range of 973-1143 cm-1 are attributed to stretching vibrations of C-O-C (glycosidic bridge) and C-O-H bonds in the AG, while the bending vibration of CH_2 emerges at 1421 cm^{-1} [32, 33, 35]. In comparison to pure AG, the FT-IR spectra of AG-g-PAN/$CuFe_2O_4$ exhibit two additional sharp bands. The nitrile functional groups of PAN grafted on the AG chain caused the first band to occur at 2243 cm^{-1}, while the stretching vibration of the Fe-O in $CuFe_2O_4$ caused the second band to form at 615 cm-1. It is hypothesized that the nitrile groups of PAN in AG-g-PAO/$CuFe_2O_4$ changed to amidoxime (H_2N–C=NOH) groups in the FT-IR spectra of AG-g-PAO/$CuFe_2O_4$. The elimination of the nitrile groups' absorption band at 2243 cm^{-1} and the emergence of a new weak absorption band verified this.

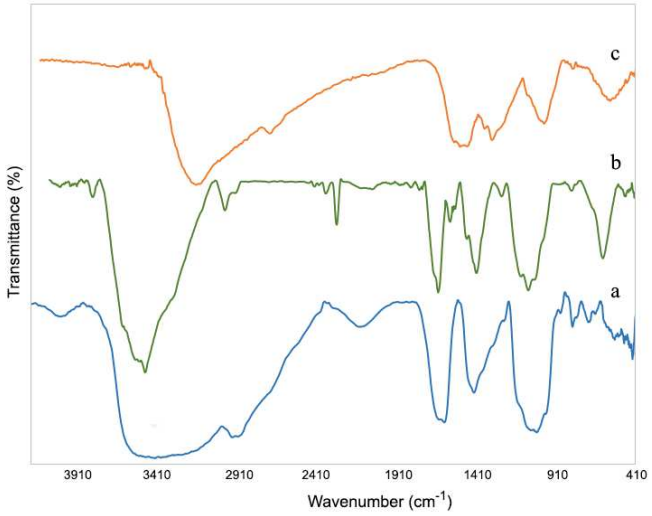

Figure 1. The FT-IR spectra of (**a**) AG, (**b**) AG-*g*-PAN/$CuFe_2O_4$, and (**c**) AG-*g*-PAO/$CuFe_2O_4$.

The EDX analysis was performed to evaluate the chemical structure and existence of the component elements of the samples qualitatively. **Figure 2** displays the results of this study for AG, AG-g-PAN, $CuFe_2O_4$, AG-g-PAO, and AG-g-PAO/$CuFe_2O_4$. In addition to the carbon and oxygen peaks, a nitrogen sharp peak was added to the EDX diagram of AG-g-PAN, which is the consequence of the copolymerization of acrylonitrile on the AG chain. The contributing elements of AG-g-PAO are comparable to those of AG-g-PAN, but peak intensities and element percentages differ. Peak intensity and weight percentages have increased, particularly for oxygen atoms. Copper, iron, and oxygen were present in $CuFe_2O_4$. The peak of iron and copper elements were also identified in the EDX spectrum of the AG-g-PAO/$CuFe_2O_4$ nanocomposite.

CHN analysis was conducted to investigate the chemical alteration of AG-g-PAN/$CuFe_2O_4$ to AG-g-PAO/$CuFe_2O_4$. **Table 1** shows the percentages of hydrogen, nitrogen, and carbon components in the two samples. In AG-g-PAN/$CuFe_2O_4$ and AG-g-PAO/$CuFe_2O_4$, the molar ratio of nitrogen to carbon rose from 0.29 to 0.56, indicating that the nitrile group was successfully converted to amidoxime.

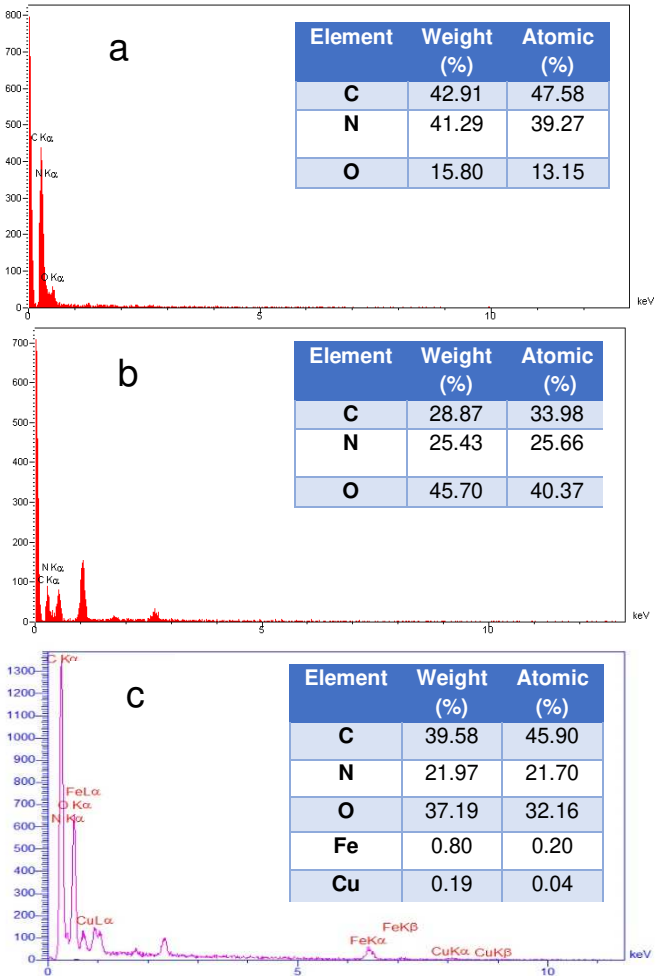

Element	Weight (%)	Atomic (%)
C	42.91	47.58
N	41.29	39.27
O	15.80	13.15

Element	Weight (%)	Atomic (%)
C	28.87	33.98
N	25.43	25.66
O	45.70	40.37

Element	Weight (%)	Atomic (%)
C	39.58	45.90
N	21.97	21.70
O	37.19	32.16
Fe	0.80	0.20
Cu	0.19	0.04

Figure 2. EDX spectra of (**a**) AG-*g*-PAN, (**b**) AG-*g*-PAO, and (**c**) AG-*g*-PAO/$CuFe_2O_4$.

Table 1. The result of elemental analysis (CHN)

Sample	C (%)	H (%)	N (%)
AG-*g*-PAN /$CuFe_2O_4$	38.75	4.02	11.12
AG-*g*-PAO/$CuFe_2O_4$	22.94	4.54	12.84

XRD analysis in the 5–80° range was used to study the crystallinity of the produced materials. The XRD pattern of AG revealed two distinct peaks at 27° and 19°, suggesting its amorphous nature, as previously described in the literature [36, 37]. As reflected in **Figure 3(I-a)**, the XRD pattern of the $CuFe_2O_4$ NPs has diffraction peaks at 2θ = 18.39º, 30.16º, 35.74º, 43.29º, 57.18º, and 62.76º, showing the crystalline nature of $CuFe_2O_4$ NPs. The XRD pattern of AG-g-PAO (**Figure 3(I-b)**) shows a semi-crystalline structure, indicating that the grafted polyamidoxime to AG has increased the crystallinity of the AG. The XRD pattern of the AG-g-PAO/$CuFe_2O_4$ biosorbent (Figure 3(I-c)) exhibits certain unique peaks at 6.67º, 18.38º, 31.82º, 42.99 º, 35.44º, 57.03º, and 62.61º, which are connected to the presence of AG and $CuFe_2O_4$ in nanocomposite hydrogel. This demonstrated that the AG-g-PAO/CuFe2O4 nanocomposite hydrogel was effectively made. Furthermore, using the Scherer equation, the average crystal size of the AG-g-PAO/CuFe2O4 nanocomposite was determined to be around 39 nm.

TGA curves of the (a) $CuFe_2O_4$ NPs, (b) AG-g-PAO, and (c) AG-g-PAO/$CuFe_2O_4$ nanocomposite in the temperature range of 50 to 800 °C with a heating rate of 10°C/min were performed and displayed in **Figure 3** to assess the thermal behavior and breakdown of the produced materials (II). The weight loss of 5% below 130 °C in the TGA curve of $CuFe_2O_4$ NPs (a) is due to the evaporation of H_2O molecules [38]. Additionally, the elimination of the hydroxyl group on the ferrite surface is attributed to the 8% weight loss from 130 to 400 °C [38, 39] and the creation

of the metal oxide phase from the degradation of nitrate waste employed as a ferrite precursor [38, 40]. A very minor weight loss with a very gradual slope happened as the temperature was increased from 400 to 600 °C, which might be attributed to the crystallization of ferrite [41]. $CuFe_2O_4$ exhibited remarkable thermal stability, with a char production of 90% at 800 °C.

The minor weight loss seen in the AG-g-PAO/$CuFe_2O_4$ nanocomposite thermogram (c) was due to the released adsorbed water in the hydrogel network and $CuFe_2O_4$ NPs structure, as well as the elimination of the remaining organic solvent. The disintegration of carboxylic acid, amidoxime functional groups in hydrogel network, decomposition of polysaccharide backbone, and also dehydroxylation of $CuFe_2O_4$ NPs surface and AG, caused the next weight loss, which began at 220 °C and proceeded with a constant trend up to 400°C [24]. Depolymerization of the main chain of grafted PAO occurred as the temperature increased from 400 to 800 °C, resulting in the degradation of the gum biopolymer chain to glucopyranose union [42].

At the end of this temperature range, the nanocomposite's residual weight was around 41%. When the TGA curves of the AG-g-PAO and AG-g-PAO/$CuFe_2O_4$ nanocomposite were compared, the AG-g-PAO lost almost 80% of its weight by 800°C, while the AG-g-PAO/$CuFe_2O_4$ nanocomposite lost 59%. As a result, the addition of $CuFe_2O_4$ NPs to its network resulted in increased heat resistance.

VSM analysis was used to evaluate the magnetic properties of (a) $CuFe_2O_4$ NPs and (b) AG-g-PAO/$CuFe_2O_4$ nanocomposite hydrogel using an applied magnetic field ranging from 10000 to +10000 Oe at ambient temperature (300 K). **Figure 3** shows that the magnetization curve of AG-g-PAO/$CuFe_2O_4$ nanocomposite has an S-like shape without remanence (Mr) or coercivity (Hc), suggesting that the AG-g-PAO/$CuFe_2O_4$ biosorbent is superparamagnetic. The synthesized biosorbent had a saturation magnetization (Ms) of about 12 emu g^{-1}, which was less than the $CuFe_2O_4$ NPs' stated value of 36.03 emu g^{-1} [43]. Given that the nanocomposite hydrogel's principal component is an organic component, this decrease is logical.

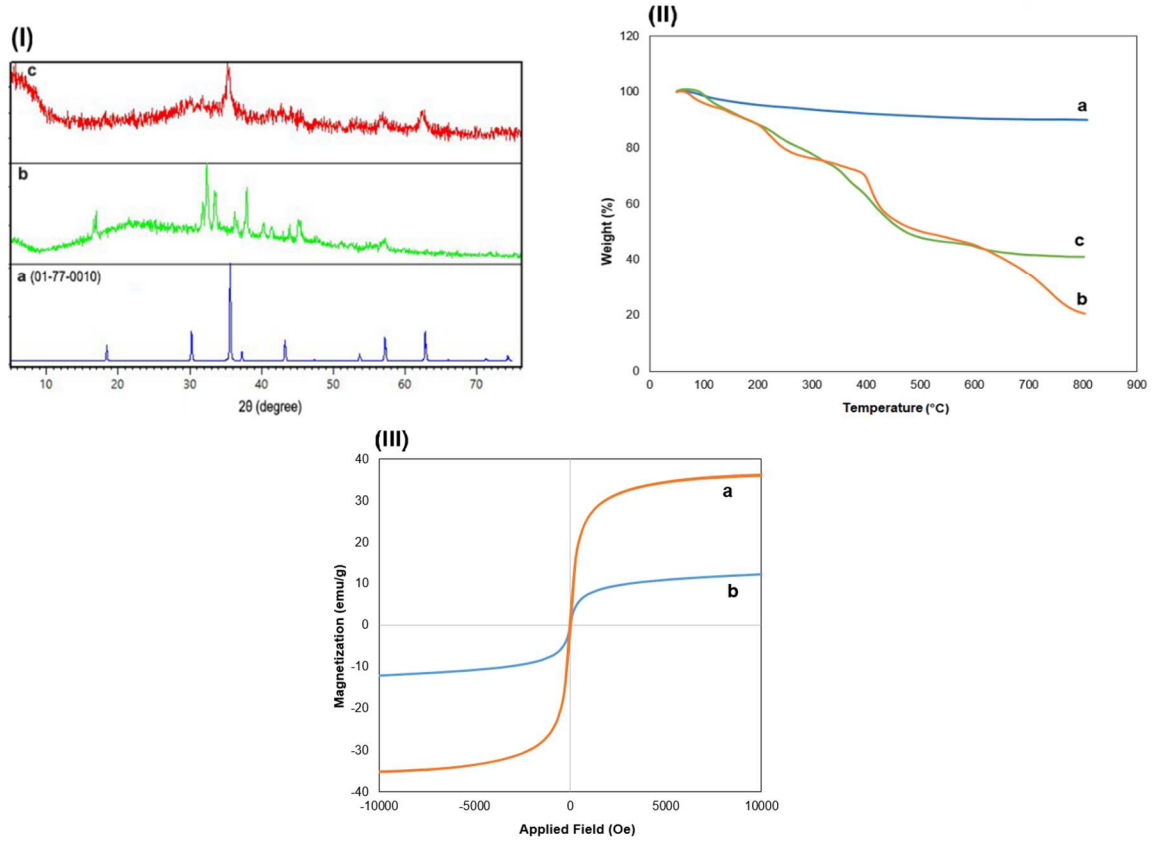

Figure 3. **(I)** XRD patterns of (a) $CuFe_2O_4$ (b) AG-*g*-PAO, and (C) AG-*g*-PAO/$CuFe_2O_4$. **(II)** the TGA analysis of (a) $CuFe_2O_4$ NPs, (b) AG-g-PAO, and (c) AG-g-PAO/$CuFe_2O_4$. **(III)** the VSM analysis of (a) $CuFe_2O_4$ NPs and (b) AG-*g*-PAO/$CuFe_2O_4$.

Surface charges of the AG-g-PAO/$CuFe_2O_4$ nanocomposite adsorbents were determined by zeta potential measurements. At pH 4, 6, and 10, the AG-g-PAO/$CuFe_2O_4$ hydrogel nanocomposite's zeta potentials were measured -12.7, -22.3, -34.1, respectively. By increasing the pH, the values of zeta potential become more negative, since hydroxyl groups, carboxylic acids, and amidoxime groups in its structure are deprotonated.

An N_2 adsorption-desorption study was performed on AG-gPAO and AG-g-PAO/$CuFe_2O_4$ samples to determine their specific surface areas and to investigate the effect of the inclusion of $CuFe_2O_4$ nanoparticles. A specific surface area of 1.033 m^2/g of AG-g-PAO/$CuFe_2O_4$ was found to be satisfactory in comparison with AG-g-PAO's 0.50 m^2/g. According to this fact, AG-g-PAO/$CuFe_2O_4$ has a greater surface area than AG-g-PAO due to the addition of $CuFe_2O_4$ to the polymeric matrix. In addition, the pore size of the AG-g-PAO/$CuFe_2O_4$ was measured to be 77.4 nm.

SEM analysis was used to examine the surface morphology and size distribution of the produced samples. **Figure 4** shows SEM micrographs of (a) $CuFe_2O_4$, (b) AG-g-PAO, and (c) AG-g-PAO/$CuFe_2O_4$ nanocomposite. SEM micrographs of AG-g-PAO (a and b) revealed round swollen topologies on the smooth surface with uniform distribution, which might be due to uniform PAO grafting onto the AG backbone. The aggregation of nearly sheet-shaped particles can be seen in the SEM pictures of $CuFe_2O_4$ (c and d), with an average particle size of 37 nm for 20 particles. When compared to AG-g-PAO, the surface morphology of AG-g-PAO/$CuFe_2O_4$ biosorbent showed noteworthy differences, with a large number of sheet-like particles scattered throughout the AG-g-PAO matrix, which appear to be connected to $CuFe_2O_4$.

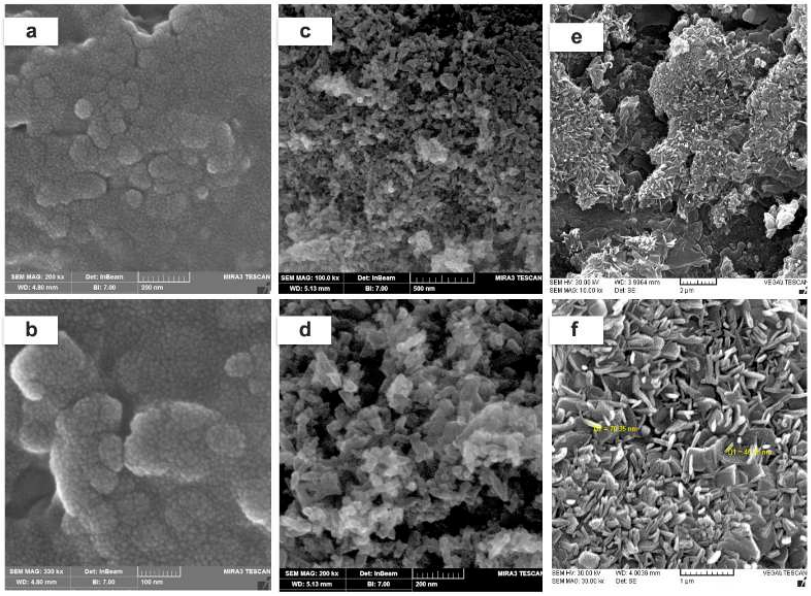

Figure 4. SEM images of (**a** and **b**) AG-*g*-PAO and (**c** and **d**) $CuFe_2O_4$ NPs and (**e** and **f**) the AG-g-PAO/$CuFe_2O_4$.

3.2. Optimization of the effective parameters on the Pb(II) adsorption

The effects of metal ion starting concentration, contact duration, adsorbent dose, and pH are significant and deciding factors. By adjusting these variables, the efficiency of heavy metal ions removal can be greatly improved [10].

Solution pH: **Figure 5a** shows the results of tests in which the pH of the aqueous solutions varied from 2 to 10. The adsorption capability of the AG-g-PAO/$CuFe_2O_4$ biosorbent is pH-dependent based on the chemical structure of chelating sites, namely amidoxime as an amide, hydroxyl, bidentate ligand, and carboxyl groups. The interactions between the active basic sites of the AG-g-PAO/$CuFe_2O_4$ biosorbent and the Pb(II) cations are influenced by the acidity and alkalinity of the metal ion solution, as well as the concentration of proton and hydroxide ions. At low pH, the active sites of the AG-*g*-PAO/$CuFe_2O_4$ are protonated and less accessible for coordination with Pb(II) cations. As **Figure 5a** shows, the concentration of Pb(II) in solution at pH 2 did not decrease after 1h stirring in the presence of the AG-*g*-PAO/$CuFe_2O_4$. This observation can be explained by the electrostatic repulsion between protonated chelating sites of the AG-*g*-PAO/$CuFe_2O_4$ and lead cations[10]. The adsorption capacity grew as the pH climbed from 2 to 6, approaching its maximum value of around 148 mg/g, but when the pH increased to 8 and 10, the adsorption

capacity marginally fell to 127 and 116 mg/g, correspondingly. The reason for this decrease in adsorption capacity at higher pH is attributed to the increase in the concentration of hydroxide ions and the formation of other species of Pb ions such as $Pb(OH)_2$ and even $Pb(OH)_3$[10]. In other words, there is a competition between the AG-*g*-PAO/$CuFe_2O_4$ biosorbent chelating sites and hydroxide ions to interact with the Pb(II) cations in an aqueous solution, so that all metal cations not are available to the adsorbent chelating sites. The pH of 6 was chosen as the ideal pH for further adsorption trials since it had the most adsorption capacity.

Adsorbent dosage: Adsorption studies were carried out in the presence of varying amounts of the AG-g-PAO/$CuFe_2O_4$ biosorbent at optimal pH to study the link between the amount of the AG-g-PAO/$CuFe_2O_4$ adsorbent and its adsorption ability for Pb(II). The amount of adsorbent steadily increased from 0.002 g to 0.014 g, while the adsorption capacity fell from 360 to 65 mg/g, in accordance with the obtained data (**Figure 5b**). The increased number of Pb(II) ions accessible for adsorption per unit mass of the AG-g-PAO/$CuFe_2O_4$ biosorbent results in a higher amount of adsorption capacity at a lower adsorbent dose. However, when the amount of adsorbent was increased, the adsorption efficiency increased since the swelling and availability of a greater number of active sites with an increase in the dose of absorbent. When the adsorbent dose was 0.014 g, the greatest adsorption effectiveness was around 91 percent. Therefore, 0.014 is the best quantity of adsorbent for the following studies.

Contact time: The effect of contact time on the AG-g-PAO/$CuFe_2O_4$ biosorbent's adsorption ability for the removal of Pb (II) was examined. **Figure 5c** shows that increasing the contact period from 30 to 90 minutes at the optimal pH and adsorbent dose raised the adsorption capacity to 69.22 mg/g. However, as the response time approaches 120 minutes, the adsorption capacity does not improve and even slightly declines. As a result of the research, the best contact period for future experiments is 90 minutes. A significant number of unoccupied chelating sites of biosorbent are accessible to coordinate with metal cation in an aqueous solution at the start of the metal ion adsorption process. The interactions between adsorbent chelating sites and metal ions grow when the contact duration is increased to 90 minutes, till the highest equilibrium adsorption capacity is reached. However, no increase in adsorption capacity was found after this period, which could be interpreted by the occupancy of the AG-g-PAO/$CuFe_2O_4$ biosorbent active sites and the proximity to equilibrium.

The initial concentration of Pb(II) ions: By adjusting Pb(II) ions concentration from 25 to 200 mg/L at optimal pH (6), adsorbent dose (0.014 g), and contact duration (90 min), the relationship between initial metal ions concentration and adsorption capacity of the AG-g-PAO/$CuFe_2O_4$ biosorbent was investigated. The initial concentration of Pb(II) influenced the biosorbent adsorption capacity (**Figure 5d**), and the severity of the effect increased as the initial concentration rose from 25 to 200 mg/L. Moreover, raising the starting concentration of Pb(II) ions while keeping the quantity of adsorbent constant improved the ratio of adsorbate to the adsorbent, resulting in an increase in adsorption capacity until it approaches an equilibrium level[44].

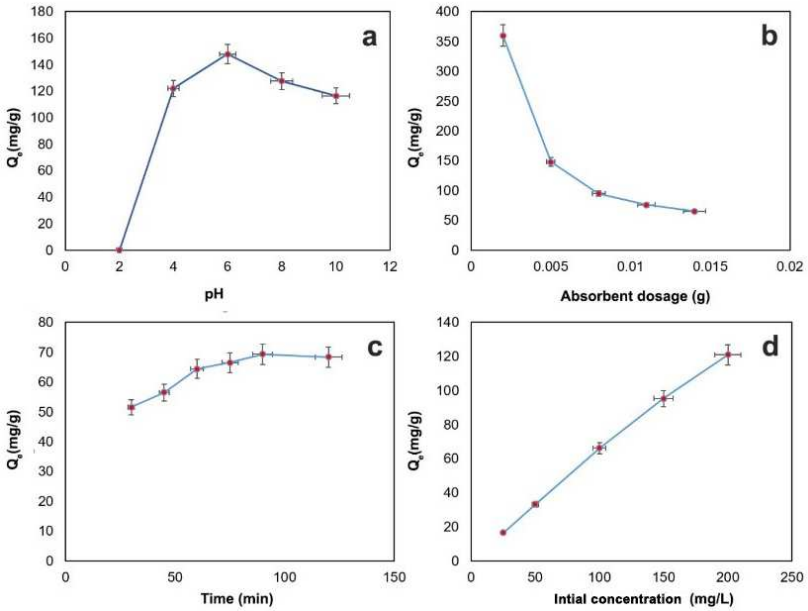

Figure 5. (**a**) Effect of solution pH (2–10), adsorbent dosage (0.010 g), initial concentration (100 mg/L), V (10 mL), Time (60 min), T (298 K), (**b**) adsorbent dosage (0.02–0.014 g), pH 6, initial concentration (100 mg/L), V (10 mL), Time (60 min), T (298 K), (**c**) contact time (30–120 min), pH 6, adsorbent dosage (0.014 g), initial concentration (100 mg/L), V (10 mL), Time (60 min), T (298 K), (**d**) initial concentration (50-200 mg/L), pH 6, adsorbent dosage (0.014 g), V (10 mL), Time (90 min), T (298 K). Qe is the equilibrium adsorption capacity (mg/g).

3.3. Adsorption isotherm

The adsorption isotherm investigation was used to investigate how Pb(II) interacts with AG-g-PAO/$CuFe_2O_4$ biosorbent. In recent years, Langmuir and Freundlich's models have been used to describe equilibrium adsorption isotherms and predict maximum adsorption capacity [10, 11, 45, 46]. A single-layered absorption of pollutants onto the adsorbent surface is described by the Langmuir isotherm. All sites on the adsorbent surface are assumed to have the same energy and affinity for interacting with pollutants, resulting in homogeneous adsorption [47]. Admittedly, the adsorption capacity reaches its greatest levels when contaminants form a full monolayer on the adsorbent surface [23]. The Freundlich model, on the other hand, is based on multilayer adsorption of pollutants on a heterogeneous adsorbent surface [48]. Langmuir's (4) and Freundlich's (5) models are mathematically expressed in the equations provided [11].

$$\frac{C_e}{Q_e} = \frac{1}{K_L Q_{max}} + \frac{1}{Q_{max}} C_e \quad (4)$$

$$Log Q_e = \log K_f + \frac{1}{n} \log C_e \quad (5)$$

Ce is the equilibrium concentration of metal ions (mg/L); Q_e and Q_{max} are the equilibrium and maximum adsorption capacity (mg/g), respectively; K_L (L/mg) and K_F (L/mg) are the Langmuir and Freundlich constants calculated from the plot between Ce/Q_e and Ce, and between log Q_e and log C_e, respectively. n is a factor to determine the favorability of the adsorption process; when n>1, At high concentrations, adsorption of Pb(II) on adsorbent is ideal [45]. **Figure 6** provides the charts for the Langmuir and Freundlich isotherm models. **Table 2** presents the comprehensive information acquired from these two isotherms. The Langmuir isotherm is highly compatible with experimental results than the Langmuir isotherm, showing monolayer adsorption of metal ions onto the homogeneous surface of the AG-g-PAO/$CuFe_2O_4$ biosorbent, according to the corresponding correlation coefficient (R2) of isotherm models. The obtained biosorbent's highest adsorption capacity for Pb (II) is 192.30 mg/g when compared to some of the other biosorbents published in recent years to demonstrate the prepared biosorbent's competence. The AG-g-PAO/$CuFe_2O_4$ biosorbent has a higher Qmax than other published biosorbents, as seen in **Table 3**. This is due to the presence of several chelating agents in the copolymer, such as hydroxyl, amine, and amidoxime functional groups, as well as

$CuFe_2O_4$ NPs in the produced nanocomposite hydrogel network, where it has a significant affinity for the building of a stable Pb(II) complex in aqueous solution. Therefore, the AG-g-PAO/$CuFe_2O_4$ biosorbent is a good option for successful heavy metal ion adsorption from wastewater.

Table 2. Isotherm and kinetic constants, correlation coefficients, and statistical parameters, for adsorption of Pb(II) on the adsorbent.

		Parameters	
Isotherm	Langmuir	q_m (mg/g)	192.30
		K_L(L/mg)	0.058
		R^2	0.97
	Freundlich	K_f (L/mg)	12.65
		n	1.41
		R^2	0.95
Kinetics	Pseudo-first-order	K_1	0.0345
		$Q_{e, exp}$ (mg/g)	69.29
		$Q_{e, cal}$ (mg/g)	45.18
		R^2	0.962
	Pseudo-second-order	K_2	0.0007
		$Q_{e, exp}$ (mg/g)	69.29
		$Q_{e, cal}$ (mg/g)	76.92
		R^2	0.99

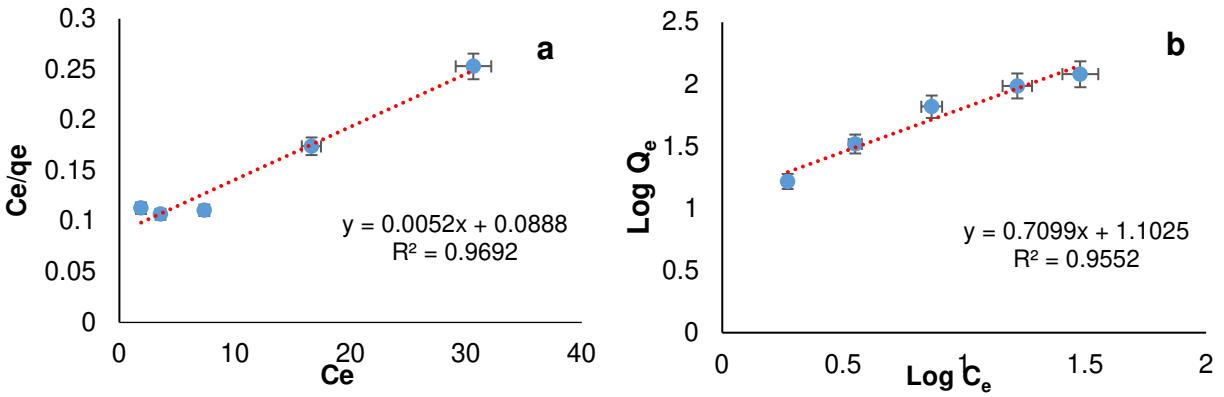

Figure 6. (**a**) The Langmuir and (**b**) Freundlich isotherm (Condition: initial concentration (50–200 mg/L), pH 6, adsorbent dosage (0.014 g), contact time (90 min), T (298 K).

Table 3. Comparison of the adsorption capacities of various adsorbents for Pb(II) adsorption.

Adsorbents	Q_{max} (mg/g)	pH	Time (min)	C (mg/L)	m (mg)	Ref.
Guar gum/bentonite	83.52	5.1	240	50	10	[49]
Wool graft polyacrylamidoxim	23.56	6	720	20	200	[50]
magnetic PVA/modified GT/GO beads	81.78	6	24h	20	50	[51]
Poly m-phenylenediamine- grafted -dextrin	80	6	120	80	120	[10]
Xanthangum/montmorillonite	187.08	4	240	100	10	[52]
Magnetic chitosan grafted thiacalix[4]arene	23.28	7	240	50	50	[11]
AG-*g*-PAO/$CuFe_2O_4$	192.30	6	90	200	140	Present work
$CuFe_2O_4$	39.54	6	90	200	140	Present work
AG-*g*-PAO	156.25	6	90	200	140	Present work

3.4. Adsorption kinetics

The investigation and determination of various adsorption processes, the rate-limiting stage of the adsorption process, and the equilibrium time can all be done using adsorption kinetics [53]. The adsorption rates of Pb(II) onto the AG-g-PAO/$CuFe_2O_4$ biosorbent were assessed using pseudo-first-order and pseudo-second-order models in this work. Equations 6 and 7 are used to represent them mathematically, accordingly [46].

$$Log(Q_e - Q_t) = LogQ_e - \frac{k_1}{2.303}t \quad (6)$$

$$\frac{t}{Q_t} = \frac{1}{k_2 Q_e^2} + \frac{1}{Q_e}t \quad (7)$$

The adsorption capacity (or quantity of Pb(II) adsorbed onto biosorbent) at time and equilibrium, accordingly, are Qt (mg/g) and Q_e(mg/g). The pseudo-first-order and pseudo-second-order rate constants are K_1 (1/min) and K_2 (g/mg.min), accordingly. **Figure 7** and **Table 2** present the results of the kinetic linear plots and their full information pseudo-second-order model is better adequate for understanding Pb(II) adsorption kinetics on the AG-g-PAO/$CuFe_2O_4$ biosorbent, based on the correlation coefficients and discrepancy between the predicted and observed Qe values of the two analyzed kinetic models. As a result, chemisorption, which includes a coordination bond between the metal ion and the chelating ligands of the adsorbent, is the rate-limiting stage of the Pb(II) adsorption process on biosorbent.

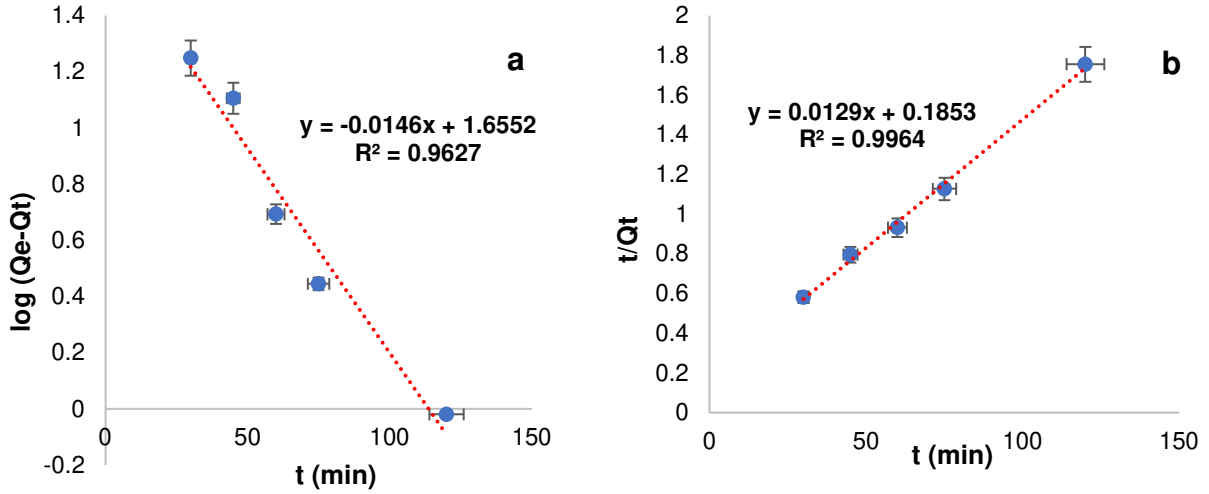

Figure 7. (**a**) The pseudo-first-order (**b**) and pseudo-second-order models (Conditions: Contact time (30-120), pH:6, adsorbent dosage (0.014 g), initial concentration (100 mg/L), T (298 K).

3.5. Recovery and reusability

Adsorbent retrievability and recyclability are essential for the protection of the environment and expense, time, and energy efficiency since adsorbents with these features effectively decrease the challenges associated with old adsorbent waste and even the current adsorbent manufacturing process [54]. Three cycles of adsorption and desorption experiments were conducted to determine the AG-g-PAO/$CuFe_2O_4$ biosorbent's reusability. Under acidic conditions (HCl 2M), the coordination bond between the metal cation and the biosorbent was broken, releasing the metal ion into the acidic solution. The adsorbent was then isolated first by a magnet, washed several times with distilled water, and dried for subsequent adsorption/desorption experiments. **Figure 8a** shows that after three cycles, the adsorption percentage dropped from 97.01% to 93.98%, whereas the desorption percentage dropped from 96.2% to 92.87%. These findings reveal that the biosorbent keeps its capacity to remove metal ions through three adsorption-desorption cycles with no substantial loss of adsorption efficacy.

3.6. Suggested mechanisms of adsorption

Absorption of Pb(II) on AG-*g*-PAO/$CuFe_2O_4$ biosorbent was demonstrated by EDX analysis of biosorbent before and after adsorption of Pb(II). The functional groups and chemical structure of the adsorbent are significant in the process of adsorption. The AG-*g*-PAO/$CuFe_2O_4$ nanocomposite hydrogel, with its large number of chelating groups such as carboxyl, hydroxyl, and amidoxime groups and also the three-dimensional network, has a very excellent ability to adsorb lead ions from aqueous solution. To confirm the adsorption of Pb(II) on the AG-*g*-PAO/$CuFe_2O_4$, EDX analysis was employed. In this way, the biosorbent was analyzed before and after the adsorption of Pb(II). Comparing the EDX spectrum of the AG-*g*-PAO/$CuFe_2O_4$ hydrogel biosobent before and after adsorption (**Figure 8b** and **Figure 8c)**, showed that new peaks related to lead element were present in the EDX spectrum of biosobent after adsorption.

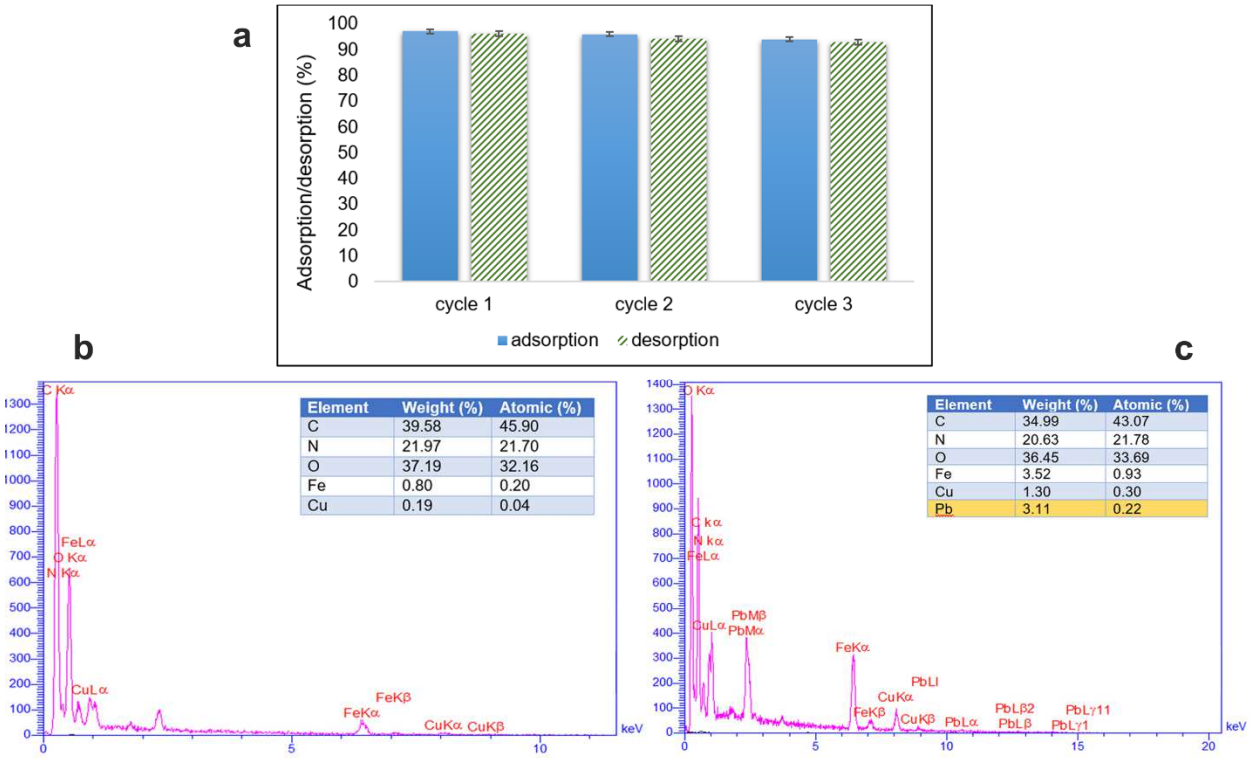

Figure 8. (a) Reusability of the AG-*g*-PAO/$CuFe_2O_4$ adsorption/desorption percentages of Pb(II) during three cycles. (Reaction conditions: contact time (90 min), solution pH:6, adsorbent dosage (0.014g), Initial concentration (100 mg/L) solution volume: 10 mL. T (298 K). (b, c) EDX spectra of the AG-*g*-PAO/$CuFe_2O_4$ nanocomposite hydrogel before and after Pb(II) adsorption.

4. Conclusions

In three main processes, the AG-g-PAO/$CuFe_2O_4$ nanocomposite was developed as a unique organic/inorganic hydrogel, and it was analyzed with FTIR, CHN, and EDX, SEM, XRD, TGA, and VSM analyses. The adsorption of Pb(II) from an aqueous solution was accomplished when using AG-g-PAO/$CuFe_2O_4$ nanocomposite hydrogel. The best conditions for Pb(II) adsorption onto AG-g-PAO/$CuFe_2O_4$ were 200 mg/L starting concentration of Pb(II), 0.014 mg adsorbent dosage, and 90 minutes contact time at pH=6. The adsorption isotherm data were matched with a Langmuir isotherm model having a Q_{max} of 192.30 mg/g, and the experimental adsorption kinetics were well aligned to pseudo-second-order and adsorption isotherm data. The creation of a stable complex between the chelating ligands of the adsorbent network, namely amidoxime (as a bidentate ligand), hydroxyl, amidoxime, carboxyl groups, and Pb(II), can clarify the process of metal adsorption on the hydrogel network. The AG-g-PAO/$CuFe_2O_4$ biosorbent had better thermal stability than AG-g-PAO and lower thermal stability than $CuFe_2O_4$ NPs. Moreover, the existence of $CuFe_2O_4$ NPs in the AG-g-PAO hydrogel network enabled the creation of a recyclable magnetic hydrogel that could be easily removed from aqueous solutions. After three sequential cycles, the synthetic adsorbent's high ability to

absorb Pb(II) was only diminished by around 4%. Considering the aforementioned merits of this nanocomposite hydrogel, more research is certainly possible, including using it as a photocatalyst for the degradation of organic pollutants and examining its catalytic performance for organic reactions and its antibacterial properties.

Authors' contributions

All authors contributed to data analysis, drafting and revising of the paper and agreed to be responsible for all the aspects of this work.

Acknowledgments

All authors kindly acknowledge the Research Council of Iran University of Science and Technology for providing partial funding.

Declaration of competing interest

The authors declare no competing interest.

Funding

This paper received no external funding.

Data availability

Data will be made available on request.

References

[1] E. Alizadeh, H. Baseri, Photocatalytic degradation of Sumatriptan Succinate by ZnO, Fe doped ZnO, and TiO_2-ZnO nanocatalysts, Mater. Chem. Horizons., 1(1) (2022) 7–21.
[2] A. Mehdizadeh, P. Najafi Moghadam, S. Ehsanimehr, A.R. Fareghi, Preparation of a New Magnetic Nanocomposite for the Removal of Dye Pollutions from Aqueous Solutions: Synthesis and Characterization, Mater. Chem. Horizons., 1(1) (2022) 23–34.
[3] V. Srivastava, E.N. Zare, P. Makvandi, X.-q. Zheng, S. Iftekhar, A. Wu, V.V. Padil, B. Mokhtari, R.S. Varma, F.R. Tay, Cytotoxic aquatic pollutants and their removal by nanocomposite-based sorbents, Chemosphere, 258 (2020) 127324.
[4] L. Zhang, Y. Zeng, Z. Cheng, Removal of heavy metal ions using chitosan and modified chitosan: A review, J. Mol. Liq., 214 (2016) 175-191.
[5] S. Iftekhar, G. Heidari, N. Amanat, E N. Zare, M.B. Asif, M. Hassanpour, V.P. Lehto, M. Sillanpaa, Porous materials for the recovery of rare earth elements, platinum group metals, and other valuable metals: a review, Environ. Chem. Lett., (2022) https://doi.org/10.1007/s10311-022-01486-x
[6] F.B. Kheyrabadi, E.N. Zare, Antimicrobial nanocomposite adsorbent based on poly (meta-phenylenediamine) for remediation of lead (II) from water medium, Sci. Rep., 12(1) (2022) 1-14.
[7] E.J. Olguín, G. Sánchez-Galván, Heavy metal removal in phytofiltration and phycoremediation: the need to differentiate between bioadsorption and bioaccumulation, N. Biotechnol., 30 (2012) 3-8.
[8] H.N.M.E. Mahmud, A.O. Huq, R. binti Yahya, The removal of heavy metal ions from wastewater/aqueous solution using polypyrrole-based adsorbents: a review, RSC Adv., 6 (2016) 14778-14791.
[9] H. Mittal, A. Maity, S.S. Ray, Synthesis of co-polymer-grafted gum karaya and silica hybrid organic–inorganic hydrogel nanocomposite for the highly effective removal of methylene blue, Chem. Eng. J., 279 (2015) 166-179.
[10] E.N. Zare, M.M. Lakouraj, N. Kasirian, Development of effective nano-biosorbent based on poly m-phenylenediamine grafted dextrin for removal of Pb (II) and methylene blue from water, Carbohydr. Polym., 201 (2018) 539-548.
[11] M.M. Lakouraj, F. Hasanzadeh, E.N. Zare, Nanogel and super-paramagnetic nanocomposite of thiacalix [4] arene functionalized chitosan: synthesis, characterization and heavy metal sorption, Iran. Polym. J., 23 (2014) 933-945.
[12] R. Sharma, B.S. Kaith, S. Kalia, D. Pathania, A. Kumar, N. Sharma, R.M. Street, C. Schauer, Biodegradable and conducting hydrogels based on Guar gum polysaccharide for antibacterial and dye removal applications, J. Environ. Manage., 162 (2015) 37-45.
[13] H. Mittal, A. Maity, S.S. Ray, Gum karaya based hydrogel nanocomposites for the effective removal of cationic dyes from aqueous solutions, Appl. Surf. Sci. , 364 (2016) 917-930.
[14] E. Makhado, S. Pandey, P.N. Nomngongo, J. Ramontja, Preparation and characterization of xanthan gum-cl-poly (acrylic acid)/o-MWCNTs hydrogel nanocomposite as highly effective re-usable adsorbent for removal of methylene blue from aqueous solutions, J. Colloid Interface Sci., 513 (2018) 700-714.

[15] H. Mittal, A. Maity, S.S. Ray, Effective removal of cationic dyes from aqueous solution using gum ghatti-based biodegradable hydrogel, Int. J. Biol. Macromol., 79 (2015) 8-20.
[16] R. Sahraei, M. Ghaemy, Synthesis of modified gum tragacanth/graphene oxide composite hydrogel for heavy metal ions removal and preparation of silver nanocomposite for antibacterial activity, Carbohydr. Polym., 157 (2017) 823-833.
[17] J. Ma, G. Zhou, L. Chu, Y. Liu, C. Liu, S. Luo, Y. Wei, Efficient removal of heavy metal ions with an EDTA functionalized chitosan/polyacrylamide double network hydrogel, ACS Sustain. Chem. Eng. , 5 (2017) 843-851.
[18] R.R. Mohamed, M.H.A. Elella, M.W. Sabaa, Cytotoxicity and metal ions removal using antibacterial biodegradable hydrogels based on N-quaternized chitosan/poly (acrylic acid), Int. J. Biol. Macromol. , 98 (2017) 302-313.
[19] A. Islam, G. Phillips, A. Sljivo, M. Snowden, P. Williams, A review of recent developments on the regulatory, structural and functional aspects of gum arabic, Food Hydrocoll., 11 (1997) 493-505.
[20] Y. Manawi, G. McKay, N. Ismail, A.K. Fard, V. Kochkodan, M.A. Atieh, Enhancing lead removal from water by complex-assisted filtration with acacia gum, Chem. Eng. J., 352 (2018) 828-836.
[21] E. Abdel-Bary, A. Elbedwehy, Graft copolymerization of polyacrylic acid onto Acacia gum using erythrosine–thiourea as a visible light photoinitiator: Application for dye removal, Polym. Bull., 75 (2018) 3325-3340.
[22] V.V. Padil, S. Wacławek, M. Černík, R.S. Varma, Tree gum-based renewable materials: Sustainable applications in nanotechnology, biomedical and environmental fields, Biotechnol. Adv., 36 (2018) 1984-2016.
[23] A. Masoumi, M. Ghaemy, Removal of metal ions from water using nanohydrogel tragacanth gum-g-polyamidoxime: isotherm and kinetic study, Carbohydr. Polym., 108 (2014) 206-215.
[24] M.L. Rahman, C.J. Fui, M.S. Sarjadi, S.E. Arshad, B. Musta, M.H. Abdullah, S.M. Sarkar, E.J. O'Reilly, Poly (amidoxime) ligand derived from waste palm fiber for the removal of heavy metals from electroplating wastewater, Environ. Sci. Pollut., 27 (2020) 34541-34556.
[25] K. Saeed, S. Haider, T.-J. Oh, S.-Y. Park, Preparation of amidoxime-modified polyacrylonitrile (PAN-oxime) nanofibers and their applications to metal ions adsorption, J. Membr. Sci., 322 (2008) 400-405.
[26] J. Tan, Y. Song, X. Huang, L. Zhou, Facile functionalization of natural peach gum polysaccharide with multiple amine groups for highly efficient removal of toxic hexavalent chromium (Cr (VI)) ions from water, ACS omega, 3 (2018) 17309-17318.
[27] L. Zeng, Q. Liu, M. Lu, E. Liang, G. Wang, W. Xu, Modified natural loofah sponge as an effective heavy metal ion adsorbent: Amidoxime functionalized poly (acrylonitrile-g-loofah), Chem. Eng. Res. Des., 150 (2019) 26-32.
[28] S. Tao, F. Gao, X. Liu, O.T. Sørensen, Preparation and gas-sensing properties of $CuFe_2O_4$ at reduced temperature, Mater. Sci. Eng. B, 77 (2000) 172-176.
[29] F. Hassanzadeh-Afruzi, A. Maleki, E.N. Zare, Efficient remediation of chlorpyrifos pesticide from contaminated water by superparamagnetic adsorbent based on Arabic gum-grafted-polyamidoxime, Int. J. Biol. Macromol., 203 (2022) 445-456.
[30] F. Hassanzadeh-Afruzi, A. Maleki, E.N. Zare, Novel eco-friendly acacia gum-grafted-polyamidoxime@ copper ferrite nanocatalyst for synthesis of pyrazolopyridine derivatives, Journal of Nanostructure in Chemistry, (2022) 1-12.
[31] M.J. Zohuriaan-Mehr, Z. Motazedi, K. Kabiri, A. Ershad-Langroudi, New super-absorbing hydrogel hybrids from gum arabic and acrylic monomers, J. Macromol. Sci. Pure App.l Chem., 42 (2005) 1655-1666.
[32] K. Juby, C. Dwivedi, M. Kumar, S. Kota, H. Misra, P. Bajaj, Silver nanoparticle-loaded PVA/gum acacia hydrogel: Synthesis, characterization and antibacterial study, Carbohydr. Polym., 89 (2012) 906-913.
[33] M. Alang, J. Barminas, B. Aliyu, S. Osemeahon, Synthesis and optimization of polyacrylamide and gum arabic graft copolymer, Int. J. Biol. Macromol. , 5 (2011) 1694-1702.
[34] F. Zonatto, E.C. Muniz, E.B. Tambourgi, A.T. Paulino, Adsorption and controlled release of potassium, phosphate and ammonia from modified Arabic gum-based hydrogel, Int. J. Biol. Macromol., 105 (2017) 363-369.
[35] A.G. de Souza, C.T. Cesco, G.F. de Lima, S.E. Artifon, D.d.S. Rosa, A.T. Paulino, Arabic gum-based composite hydrogels reinforced with eucalyptus and pinus residues for controlled phosphorus release, Int. J. Biol. Macromol. , 140 (2019) 33-42.
[36] S. Hindi, M.O. Albureikan, A.A. Al-Ghamdi, H. Alhummiany, M.S. Ansari, Synthesis, characterization and biodegradation of gum Arabic-based bioplastic membranes, Nanosci. Nanotechnol., 4 (2017) 32-42.
[37] H.E. Emam, Arabic gum as bio-synthesizer for Ag–Au bimetallic nanocomposite using seed-mediated growth technique and its biological efficacy, J. Polym. Environ. , 27 (2019) 210-223.
[38] P. Rezaei, M. Rezaei, F. Meshkani, Low temperature CO oxidation over mesoporous iron and copper mixed oxides nanopowders synthesized by a simple one-pot solid-state method, Process Saf. Environ. Prot., 119 (2018) 379-388.
[39] J.K. Rajput, P. Arora, G. Kaur, M. Kaur, CuFe2O4 magnetic heterogeneous nanocatalyst: Low power sonochemical-coprecipitation preparation and applications in synthesis of 4H-chromene-3-carbonitrile scaffolds, Ultrason. Sonochem., 26 (2015) 229-240.
[40] M.J. Iqbal, N. Yaqub, B. Sepiol, B. Ismail, A study of the influence of crystallite size on the electrical and magnetic properties of $CuFe_2O_4$, Mater. Res. Bull., 46 (2011) 1837-1842.
[41] E. Agouriane, B. Rabi, A. Essoumhi, A. Razouk, M. Sahlaoui, B. Costa, M. Sajieddine, Structural and magnetic properties of $CuFe_2O_4$ ferrite nanoparticles synthesized by co-precipitation, J. Mater. Environ. Sci., 7 (2016) 4116-4120.
[42] J. Li, J. Wang, W. Wang, X. Zhang, Symbiotic Aerogel Fibers Made via In-Situ Gelation of Aramid Nanofibers with Polyamidoxime for Uranium Extraction, Molecules, 24 (2019) 1821.
[43] J. Feng, L. Su, Y. Ma, C. Ren, Q. Guo, X. Chen, $CuFe_2O_4$ magnetic nanoparticles: A simple and efficient catalyst for the reduction of nitrophenol, Chem. Eng. J., 221 (2013) 16-24.

[44] V. Sharma, P. Rekha, P. Mohanty, Nanoporous hypercrosslinked polyaniline: An efficient adsorbent for the adsorptive removal of cationic and anionic dyes, J. Mol. Liq., 222 (2016) 1091-1100.
[45] F. Arshad, M. Selvaraj, J. Zain, F. Banat, M.A. Haija, Polyethylenimine modified graphene oxide hydrogel composite as an efficient adsorbent for heavy metal ions, Sep. Purif. Technol., 209 (2019) 870-880.
[46] N.K. Gupta, A. Sengupta, V.G. Rane, R. Kadam, Amide-mediated enhancement of sorption efficiency of trivalent f-elements on functionalized carbon nanotube: evidence of physisorption, Sep. Sci. Technol., 52 (2017) 2049-2061.

[47] H.S. Ibrahim, T.S. Jamil, E.Z. Hegazy, Application of zeolite prepared from Egyptian kaolin for the removal of heavy metals: II. Isotherm models, J. Hazard. Mater., 182 (2010) 842-847.
[48] S.-W. Lv, J.-M. Liu, C.-Y. Li, N. Zhao, Z.-H. Wang, S. Wang, A novel and universal metal-organic frameworks sensing platform for selective detection and efficient removal of heavy metal ions, Chem. Eng. J., 375 (2019) 122111.
[49] R. Ahmad, A. Mirza, Synthesis of Guar gum/bentonite a novel bionanocomposite: isotherms, kinetics and thermodynamic studies for the removal of Pb (II) and crystal violet dye, J. Mol. Liq., 249 (2018) 805-814.
[50] C. Cao, H. Kang, N. Che, Z. Liu, P. Li, C. Zhang, W. Li, R. Liu, Y. Huang, Wool graft polyacrylamidoxime as the adsorbent for both cationic and anionic toxic ions from aqueous solutions, RSC Adv., 4 (2014) 60609-60616.
[51] R. Sahraei, Z.S. Pour, M. Ghaemy, Novel magnetic bio-sorbent hydrogel beads based on modified gum tragacanth/graphene oxide: removal of heavy metals and dyes from water, J. Clean. Prod. , 142 (2017) 2973-2984.
[52] A. Mirza, R. Ahmad, Novel recyclable (Xanthan gum/montmorillonite) bionanocomposite for the removal of Pb (II) from synthetic and industrial wastewater, Environ. Technol. Innov., 11 (2018) 241-252.
[53] S.P. Verma, B. Sarkar, Simultaneous removal of Cd (II) and p-cresol from wastewater by micellar-enhanced ultrafiltration using rhamnolipid: Flux decline, adsorption kinetics and isotherm studies, J. Environ. Manage., 213 (2018) 217-235.
[54] S. Kulkarni, J. Kaware, Regeneration and recovery in adsorption-a review, Int. J. Innov. Res. Sci. Eng. Technol., 1 (2014) 61-65.